Inorganic Chemistry

Article

pubs.acs.org/IC

Synthesis and Selective Topochemical Fluorination of the Cation and Anion-Vacancy Ordered phases Ba_2YCoO_5 and $Ba_3YCo_2O_{7.5}$

Kun Luo,[†] T. Thao Tran,[‡] P. Shiv Halasyamani,[§] and Michael A. Hayward*[,†]

[†]Department of Chemistry, Inorganic Chemistry Laboratory, University of Oxford, South Parks Road, Oxford, OX1 3QR, United Kingdom

[‡]Department of Chemistry, University of Houston, 136 Fleming Building, Houston, Texas 77204-5003, United States

[§]Department of Chemistry, Aalto University, Kemistintie, 1, 02150 Espoo, Finland

Supporting Information

ABSTRACT: The synthesis and characterization of two cation-ordered, anion-vacancy ordered phases, Ba_2YCoO_5 and $Ba_3YCo_2O_{7.5}$, is described. Neutron powder diffraction data reveal both phases adopt structures in which octahedral Y^{3+} and tetrahedral Co^{3+} centers are ordered within a "cubic" perovskite lattice. The unusual ordered pattern adopted by the cations can be attributed to the large concentration of anion vacancies within each phase. Reaction of Ba_2YCoO_5 with CuF_2 under flowing oxygen topochemically inserts fluorine into the host material to form $Ba_2YCoO_5F_{0.42(1)}$. In contrast Ba_2YCoO_5 does not intercalate oxygen, even under high oxygen pressure. The selective insertion of fluorine, but not oxygen, into Ba_2YCoO_5 is discussed and rationalized on the basis of the lattice strain of the resulting oxidized materials. Magnetization and neutron diffraction data reveal $Ba_3YCo_2O_{7.5}$ and $Ba_2YCoO_5F_{0.42}$ adopt antiferromagnetically ordered states at low-temperature, while in contrast Ba_2YCoO_5 shows no sign of long-range magnetic order.

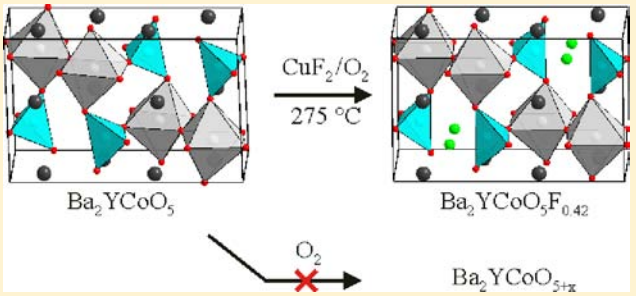

INTRODUCTION

Complex transition metal oxide phases have attracted enduring attention because of the wide variety of physical properties they exhibit.[1,2] Of particular interest are materials based on the ABO_3 cubic perovskite structure because this framework can accommodate a wide variety of different cations, on the 12-coordinate A-site and 6-coordinate B-site, and in addition phases of this type can tolerate a high degree of oxygen nonstoichiometry. This flexible chemistry gives chemists a large amount of freedom to prepare new phases and modify existing materials.

An important subset of transition metal perovskite oxides are phases which exhibit cation order.[3,4] These materials have two or more different cations on either the A- or B-sites of the perovskite lattice, and significantly these different cations are arranged into an ordered pattern throughout the extended oxide framework. Interest in these materials has been driven by the observation that cation ordered phases can exhibit physical properties which are significantly different from cation disordered analogues. For example cation ordered Sr_2FeMoO_6 exhibits half-metallic ferromagnetic behavior, while cation disordered $SrFe_{0.5}Mo_{0.5}O_3$ does not.[5]

Despite the interest in cation ordered perovskite phases, their synthesis remains a challenge, principally because at the high synthesis temperatures generally required to prepare complex oxide phases, entropy plays a dominant role in determining the structure of reaction products and strongly favors disordered cation configurations. Recently we and others have utilized the differing coordination preferences of different cations to prepare materials with complex arrangements of ordered cations in the presence of large numbers of oxygen vacancies.[6−9] Not only do phases of this type exhibit complex cation-ordered and anion-vacancy ordered structures, but if they contain oxidizable transition metals, the large concentration of anion vacancies allows additional anions to be topochemically inserted into these materials to yield further new phases with modified properties. Thus $Ba_4CaFe_3O_{9.5}$ and Ba_2YFeO_5 (Figure 1) can be oxidized with oxygen to form $Ba_4CaFe_3O_{10.4}$ and $Ba_2YFeO_{5.5}$ respectively.[7,10] In the case of $Ba_2YFeO_{5.5}$ the topochemical insertion of oxygen breaks the inversion symmetry of the host lattice, allowing second harmonic generation and pyroelectric behavior to be exhibited.

Here we describe two new cation-ordered and anion-vacancy ordered phases Ba_2YCoO_5 and $Ba_3YCo_2O_{7.5}$ and describe the formation of $Ba_2YCoO_5F_{0.42}$ via the selective insertion of fluorine in the presence of oxygen.

EXPERIMENTAL SECTION

Synthesis. Samples of $Ba_nYCo_{n-1}O_{2.5n}$ (n = 2 or 3) were prepared via a citrate precursor method. Suitable ratios of $BaCO_3$ (99.997%), Y_2O_3 (99.998%, dried at 900 °C), and cobalt powder (99.99%) were

Received: September 17, 2013
Published: November 14, 2013

   dx.doi.org/10.1021/ic402349r | Inorg. Chem. 2013, 52, 13762−13769

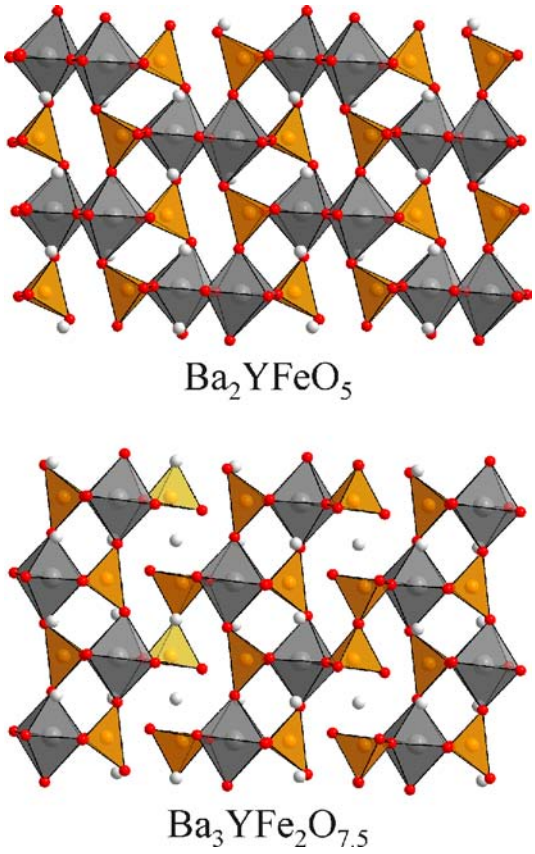

Figure 1. Anion-vacancy ordered and cation ordered structures of Ba_2YFeO_5 and $Ba_3YFe_2O_{7.5}$. Gray octahedra represent YO_6, orange tetrahedra FeO_4, and gray spheres Ba^{2+}.

dissolved in 150 mL of a 1:1 mixture of 6 M nitric acid and distilled water. $3^1/_3$ (n = 2) or 5 (n = 3) mole equivalents of citric acid and 5 mL of analar ethylene glycol were then added, and the solution heated with constant stirring. The gels thus formed were subsequently ground into fine powders and heated to 850 °C at 1 °C min^{-1} in air. The resulting materials were then pressed into 13 mm pellets and heated at 900 °C (n = 2) or 965 °C (n = 3) for 4 periods of 40 h under flowing argon. The formation of single phase samples was confirmed by X-ray powder diffraction.

Fluorination of Ba_2YCoO_5 was carried out using CuF_2 as a solid state fluorinating agent.[11] Large samples suitable for neutron powder diffraction analysis were prepared by grinding together a 1:0.625 molar ratio of Ba_2YCoO_5:CuF_2 and then heating the mixture at 275 °C under flowing oxygen for two periods of 12 h.

The fluorination reaction utilizes CuF_2 as an in situ fluorine source, which is converted into CuO during the reaction according to scheme 1.[11]

$$MO_x + CuF_2 \xrightarrow{O_2} MO_xF_y + CuO \quad (1)$$

As a result, fluorinating materials by mixing them with CuF_2 as described above, contaminates the fluorinated product with CuO. To avoid the complications associated with CuO contamination during magnetic and optical measurements, samples suitable for characterization by these techniques were prepared in reactions in which the CuF_2 and Ba_2YCoO_5 were physically separated. To achieve this, excess CuF_2 was heated at 500 °C under flowing oxygen, and the resulting mixture of gases was then passed over a sample of Ba_2YCoO_5 which was held at 275 °C. A diagram of the reaction apparatus is given in the Supporting Information. The reaction was performed for two periods of 12 h, with intermediate regrinding.

Characterization. X-ray powder diffraction data were collected using a PANalytical X'pert diffractometer incorporating an X'celerator position-sensitive detector (monochromatic Cu Kα1 radiation). Neutron powder diffraction data were collected using the GEM diffractometer at the ISIS neutron source, U.K. Rietveld profile refinements were performed using the GSAS suite of programs.[12] Average cobalt oxidation states in all phases were determined by iodometric titration. Samples were dissolved in a dilute HCl solution containing an excess of KI, and the liberated I_2 was titrated with $Na_2S_2O_3$ solution. All titrations were performed under an argon atmosphere to prevent aerial oxidation. Magnetization data were collected in an applied field of 100 Oe using a Quantum Design MPMS SQUID magnetometer.

Powder second harmonic generation (SHG) measurements were performed on a modified Kurtz-NLO system[13,14] using a pulsed Nd:YAG laser with a wavelength of 1064 nm. A detailed description of the equipment and methodology has been published elsewhere.[15] As the powder SHG efficiency has been shown to depend strongly on particle size,[13] the reported materials were ground and sieved into distinct particle size ranges (<20, 20−45, 45−63, 63−75, 75−90, >90 μm). Relevant comparisons with known SHG materials were made by grinding and sieving crystalline α-SiO_2 and $LiNbO_3$ into the same particle size ranges. No index matching fluid was used in any of the experiments.

RESULTS

Structural and Chemical Characterization of Ba_2YCoO_5 and $Ba_3YCo_2O_{7.5}$. Iodometric titrations performed on both Ba_2YCoO_5 and $Ba_3YCo_2O_{7.5}$ indicated average cobalt oxidation states of +3, consistent with the stated compositions. Neutron powder diffraction data collected from Ba_2YCoO_5 and $Ba_3YCo_2O_{7.5}$ could be readily indexed using monoclinic unit cells (Ba_2YCoO_5: a = 12.5860(1) Å, b = 6.08289(7) Å, c = 7.8070(1) Å, β = 92.247(1)°; $Ba_3YCo_2O_{7.5}$: a = 7.966(3) Å, b = 5.973(2) Å, c = 18.298(7) Å, β = 90.994(1)°). These cells are related to the unit cell of a simple cubic perovskite phase by respective $2\sqrt{2} \times \sqrt{2} \times 2$ and $2 \times \sqrt{2} \times 3\sqrt{2}$ geometric expansions, and are thus directly analogous to the unit cells of the previously reported iron phases Ba_2YFeO_5 and $Ba_3YFe_2O_{7.5}$ respectively (Figure 1).[8] Models based on the structures of Ba_2YFeO_5 (spacegroup $P2_1/n$) and $Ba_3YFe_2O_{7.5}$ (spacegroup $P2/c$) were constructed by replacing iron with cobalt and then refined against the neutron powder diffraction data collected from Ba_2YCoO_5 and $Ba_3YCo_2O_{7.5}$ respectively. The two refinements were observed to converge rapidly and give good statistical fits (Ba_2YCoO_5: χ^2 = 2.502; $Ba_3YCo_2O_{7.5}$: χ^2 = 1.907). Refinement of the yttrium and cobalt site occupancies revealed no evidence of antisite cation disorder in either phase. Full details of the refined structures of Ba_2YCoO_5 and $Ba_3YCo_2O_{7.5}$ are given in Tables 1 and 2 respectively, with selected bond lengths in Tables 3 and 4, respectively. Observed calculated and difference plots from the refinements are shown in the Supporting Information.

Oxygenation and Fluorination of Ba_2YCoO_5. Attempts to oxidize Ba_2YCoO_5 with oxygen were carried out at both ambient pressure (reaction temperatures up to 600 °C) and under 100 atm of oxygen pressure (reaction temperatures up to 250 °C). X-ray powder diffraction and titration data indicated no oxidation reaction occurred. Raising the reaction temperature above 500 °C (1 atm O_2) or 250 °C (100 atm O_2) led to the decomposition of Ba_2YCoO_5 and formation of Ba_2CoO_4 and other poorly crystalline products.

Reaction of Ba_2YCoO_5 with CuF_2 at 275 °C under flowing oxygen yielded an orthorhombic $Ba_2YCoO_xF_y$ phase (a = 12.3138(15) Å, b = 6.0804(7) Å, c = 7.8951(9) Å). X-ray powder diffraction and chemical titration data indicated that the same product phase was prepared by reactions involving both

dx.doi.org/10.1021/ic402349r | Inorg. Chem. 2013, 52, 13762−13769

Table 1. Structural Parameters Refined against Neutron Powder Diffraction Data Collected from Ba_2YCoO_5 at Room Temperature[a]

atom	x	y	z	U_{iso} (Å^2)
Ba(1)	0.1400(1)	0.2550(6)	0.0064(2)	0.0059(3)
Ba(2)	0.1159(2)	0.2499(6)	0.5051(3)	0.0059(3)
Y(1)	0.8713(1)	0.2448(6)	0.2367(2)	0.0081(3)
Co(1)	0.9070(3)	0.2351(16)	0.7520(6)	0.0183(15)
O(1)	0.8675(1)	0.2543(6)	0.5256(3)	0.0152(3)
O(2)	0.3272(1)	0.2393(6)	0.4416(2)	0.0152(3)
O(3)	0.2316(2)	0.0396(4)	0.7555(4)	0.0096(6)
O(4)	0.5089(2)	0.0255(4)	0.2724(4)	0.0152(3)
O(5)	0.4824(2)	0.5287(4)	0.2656(4)	0.0152(3)

[a]Ba_2YCoO_5: Space group $P2_1/n$; a = 12.387(6) Å, b = 6.105(3) Å, c = 7.870(3) Å, β = 91.615(1)°, V = 594.9(8) Å^3; χ^2 = 2.502, wRp = 2.32%, Rp = 2.09%.

Table 2. Structural Parameters Refined against Neutron Powder Diffraction Data Collected from $Ba_3YCo_2O_{7.5}$ at Room Temperature[a]

atom	x	y	z	U_{iso} (Å^2)
Ba(1)	0	0.2898(6)	1/4	0.0074(2)
Ba(2)	1/2	0.3207(5)	1/4	0.0074(2)
Ba(3)	0.0179(2)	0.7515(5)	0.0882(1)	0.0074(2)
Ba(4)	0.5033(3)	0.2515(5)	0.5764(1)	0.0074(2)
Y(1)	0.2458(2)	0.2498(3)	0.4109(1)	0.0040(2)
Co(1)	0.2457(5)	0.2619(10)	0.0647(2)	0.0032(8)
Co(2)	0.2291(5)	0.7730(8)	0.2622(2)	0.0090(11)
O(1)	0	0.8002(6)	1/4	0.0214(10)
O(2)	0.0428(2)	0.7670(4)	0.6066(1)	0.0103(2)
O(3)	0.4681(2)	0.2484(5)	0.0909(1)	0.0103(2)
O(4)	0.2751(3)	0.0377(4)	0.3114(1)	0.0103(2)
O(5)	0.2516(3)	0.5379(4)	0.3351(1)	0.0103(2)
O(6)	0.2363(4)	0.4899(4)	0.4999(1)	0.0103(2)
O(7)	0.2364(4)	0.0122(3)	0.9950(1)	0.0103(2)
O(8)	0.2999(3)	0.3543(4)	0.6806(1)	0.0186(6)

[a]$Ba_3YCo_2O_{7.5}$: Space group $P2/c$; a = 7.966(3) Å, b = 5.973(2) Å, c = 18.298(7) Å, β = 90.994(1)°; χ^2 = 1.907, wRp = 1.75%, Rp = 1.71%.

Table 3. Selected Bond Lengths from the Refined Structure of Ba_2YCoO_5

cation	anion	bond (Å)	BVS
Y(1)	O(1)	2.276(3)	Y +3.22
	O(2)	2.373(2)	
	O(3)	2.156(4)	
	O(3)	2.183(4)	
	O(4)	2.269(4)	
	O(5)	2.242(4)	
Co(1)	O(1)	1.838(5)	Co +2.58
	O(2)	1.820(5)	
	O(4)	1.935(8)	
	O(5)	1.863(9)	

finely ground Ba_2YCoO_5/CuF_2 mixtures and spatially separated reactants. It should be noted that a significant molar excess of CuF_2 (>3:1) and multiple heating periods were required to prepare single phase samples when reactants were spatially separated.

Structural Characterization of $Ba_2YCoO_xF_y$. To determine the crystal structure of the $Ba_2YCoO_xF_y$ phase, a number of structural models were refined against neutron powder diffraction data collected from a sample prepared from a ground mixture of Ba_2YCoO_5 and CuF_2. Given the similarity of the neutron scattering lengths of oxygen and fluorine,[16] no attempt was made to distinguish between the two anion types at this stage of the refinement. Initially a model based on the structure of $Ba_2YFeO_{5.5}$ (the product of topochemical oxidation of Ba_2YFeO_5, space group $Pb2_1m$)[10] was refined against the diffraction data collected from $Ba_2YCoO_xF_y$; however this model gave a very poor visual and statistical fit (χ^2 = 10.5) indicating $Ba_2YFeO_{5.5}$ and $Ba_2YCoO_xF_y$ have significantly different structures. Analysis of the extinction conditions of the neutron diffraction data collected from $Ba_2YCoO_xF_y$ indicates two possible space groups for the material: $Pbn2_1$ (no. 33) or $Pbnm$ (no. 62).[17] Given the low-temperature nature of the fluorination reaction it was assumed that the ordered cation lattice of the Ba_2YCoO_5 host phase was retained in the $Ba_2YCoO_xF_y$ product; therefore models were constructed in each of the two space groups based on the refined structure of Ba_2YCoO_5, but with all the "perovskite" anion sites filled to yield an initial model stoichiometry of $Ba_2YCoO_xF_y$ ($x + y = 6$) with both yttrium and cobalt in "octahedral" coordination sites. These models were refined against the data with all atomic positional and displacement parameters optimized and in addition the occupancies of all the O/F anion sites were also refined. The models in the two different space groups refined to give very similar structures, in which the framework of the Ba_2YCoO_5 host phase was faithfully retained and an additional partially occupied anion site was added at (~0.25, ~0, 1/4). In addition the two refinements yielded very similar fitting statistics ($Pbn2_1$ χ^2 = 3.08; $Pbnm$ χ^2 = 3.06). It should be noted that $Pbnm$ is a centrosymmetric space group, while $Pbn2_1$ is noncentrosymmetric.[17] SHG measurements performed on a $Ba_2YCoO_xF_y$ sample prepared from spatially separated Ba_2YCoO_5 and CuF_2 (therefore containing no acentric CuO) exhibited no detectable SHG activity, thus the structural model in the centrosymmetric $Pbnm$ space group is preferred. Full details of the refined structure are given in Table 5, with selected bond lengths in Table 6. Observed calculated and difference plots are shown in the Supporting Information.

The structural model in Table 5 yields a sample stoichiometry of $Ba_2YCoO_xF_y$, $x + y$ = 5.42. Combining this information with the observation that during the iodometric titration of this material, the cobalt present is reduced to Co^{2+}

Table 4. Selected Bond Lengths from the Refined Structure of $Ba_3YCo_2O_{7.5}$

cation	anion	bond(Å)	BVS
Y(1)	O(2)	2.319(2)	Y +3.32
	O(3)	2.281(2)	
	O(4)	2.235(3)	
	O(5)	2.212(3)	
	O(6)	2.172(3)	
	O(7)	2.197(2)	
Co(1)	O(2)	1.807(4)	Co +2.53
	O(3)	1.831(4)	
	O(6)	1.898(6)	
	O(7)	1.963(6)	
Co(2)	O(1)	1.841(4)	Co +2.68
	O(4)	1.853(5)	
	O(5)	1.943(5)	
	O(8)	1.776(4)	

dx.doi.org/10.1021/ic402349r | Inorg. Chem. 2013, 52, 13762−13769

Table 5. Structural Parameters Refined against Neutron Powder Diffraction Data Collected from $Ba_2YCoO_5F_{0.42(1)}$ at Room Temperature[a]

atom	x	y	z	fraction	U_{iso} (Å^2)
Ba(1)	0.1248(3)	0.2508(17)	0.9981(3)	1	0.0092(6)
Y(1)	0.8724(2)	0.2439(17)	1/4	1	0.0156(9)
Co(1)	0.8989(7)	0.2470(59)	3/4	1	0.0172(29)
O(1)	0.3531(2)	0.2391(14)	0.4652(3)	1	0.0303(7)
O(2)	0.2413(8)	0.0116(21)	3/4	1	0.0239(7)
O(3)	0.4862(5)	0.5065(12)	1/4	1	0.0253(7)
O(4)	0.5005(7)	0.0140(18)	1/4	1	0.0375(7)
F	0.2451(40)	0.0189(82)	1/4	0.42(1)	0.036(6)

[a]$Ba_2YCoO_5F_{0.42}$: Space group *Pbnm*; a = 12.3138(15) Å, b = 6.0804(7) Å, c = 7.8951(9) Å, V = 591.1(2) Å^3. CuO: Space group *C*2/*c*; a = 4.656(3) Å, b = 3.419(2) Å, c = 5.120(3) Å, β = 99.3(2)°; χ^2 = 3.067 wRp = 3.23%, Rp = 2.88%.

Table 6. Selected Bond Lengths from the Refined Structure of $Ba_2YCoO_5F_{0.42}$

cation	anion	bond (Å)	BVS
Y(1)	O(1)	2 × 2.263(2)	Y+3.45
	O(2)	2.195(13)	
	O(2)	2.091(14)	
	O(3)	2.262(10)	
	O(4)	2.269(13)	
Co(1)	O(1)	2 × 1.792(4)	Co+2.82
	O(3)	1.879(31)	
	O(4)	1.918(30)	
	F	2.369(54)	
	F	2.400(55)	

taking up 4.95(23) × 10^{20} electrons/g, yields an overall sample stoichiometry of $Ba_2YCoO_5F_{0.42(2)}$.

As noted above, the X-ray and neutron scattering lengths of O^{2-} and F^- are too similar to provide sufficient scattering contrast between the two anions to allow the oxide/fluoride distribution in $Ba_2YCoO_5F_{0.42}$ to be determined directly. However it is possible to determine oxide/fluoride distributions in some oxyfluoride phases through a detailed analysis of the local anion bonding polyhedra by means of bond valence sums (BVSs).[18−20] Table 7 lists the calculated BVS values for the anion sites present in Ba_2YCoO_5 and $Ba_2YCoO_5F_{0.42}$. It can be seen that the four anion sites present in $Ba_2YCoO_5F_{0.42}$ which are retained from the structure of Ba_2YCoO_5 (O(1)−O(4)) have very similar BVS values to the analogous anion sites in the unfluorinated host phase. In contrast, the BVS of the additional anion site (F) is a little over half that of the other anion sites, consistent with the presence of a fluoride ion rather than an oxide ion. Thus we can conclude that $Ba_2YCoO_5F_{0.42}$ is formed by the simple topochemical insertion of fluoride ions into Ba_2YCoO_5, with all the added fluoride ions located in a partially filled site at (∼ 0.25, ∼0, 1/4).

Table 7. Anion BVSs Calculated from the Refined Structures of Ba_2YCoO_5 and $Ba_2YCoO_5F_{0.42}$[a]

Ba_2YCoO_5		$Ba_2YCoO_5F_{0.42}$	
anion	BVS	anion	BVS
O(1)	O −1.78	O(1)	O −1.83
O(2)	O −1.69		
O(3)	O −2.18	O(2)	O −2.17
O(4)	O −1.74	O(3)	O −1.85
O(5)	O −1.92	O(4)	O −1.78
		F	O −1.02
			F −0.79

[a]All sums calculated using the parameters for Ba^{2+}, Y^{3+}, and Co^{3+}.

As discussed in more detail below, all the fluorine-cation distances in the refined structure of $Ba_2YCoO_5F_{0.42}$ are longer than is typical (Table 6). To confirm this feature of the structure a series of models in which the inserted fluoride ions were described by multiple symmetry-related anion sites located around (∼0.25, ∼0, 0.25) were refined against the diffraction data. These "split-site" descriptions of the inserted fluoride ions yielded poorer fitting statistics than the "single-site" model and in addition, when the positions of the split-site anions were allowed to refine, they converged on the (∼0.25, ∼0, 0.25) position occupied in the single-site model, confirming the stated structure.

MAGNETIC BEHAVIOR

Ba_2YCoO_5. Magnetization data collected from Ba_2YCoO_5 (Figure 2) can be fitted to the Curie−Weiss law ($\chi = C/(T - \theta)$) in the temperature range 40 < T/K < 300 to yield values of C = 2.632(2) cm^3 K mol^{-1}, θ = −34.8(1) K, broadly in agreement with a value of C = 3 cm^3 K mol^{-1} expected for the spin-only moment of one high-spin, S = 2 Co^{3+} center per formula unit. Below T ∼ 20 K zero field-cooled and field-cooled data diverge weakly. Neutron powder diffraction data collected from Ba_2YCoO_5 at 7 K show no evidence of long-range magnetic order.

$Ba_3YCo_2O_{7.5}$. Magnetization data collected from $Ba_3YCo_2O_{7.5}$ (Figure 2) can be fitted to the Curie−Weiss law in the temperature range 65 < T/K < 300 to yield values of C = 5.949(9) cm^3 K mol^{-1}, θ = −65.0(3) K, in good agreement with a value of C = 6 cm^3 K mol^{-1} expected for the spin-only moment of two high-spin, S = 2 Co^{3+} centers per formula unit. Below this temperature zero field-cooled and field-cooled data diverge weakly, before a much stronger divergence at T ∼ 25 K. Neutron powder diffraction data collected from $Ba_3YCo_2O_{7.5}$ at 7 K exhibit additional diffraction features compared to analogous data collected at ambient temperature, indicative of magnetic order. These additional diffraction features were readily indexed using the crystallographic unit cell. The intensities of these additional diffraction features are best described using an antiferromagnetic model, in which the magnetic moments of the cobalt centers in $Y_2Co_2O_{10}\square_2$ subunits are aligned parallel to the x-axis with an ordered moment of 1.64(3) μ_B per cobalt center, as shown in Figure 3. Attempts to introduce an ordered magnetic moment to the cobalt centers in Co_2O_7 dimers resulted in this parameter refining to a value of zero within error. A representation of the

dx.doi.org/10.1021/ic402349r | Inorg. Chem. 2013, 52, 13762−13769

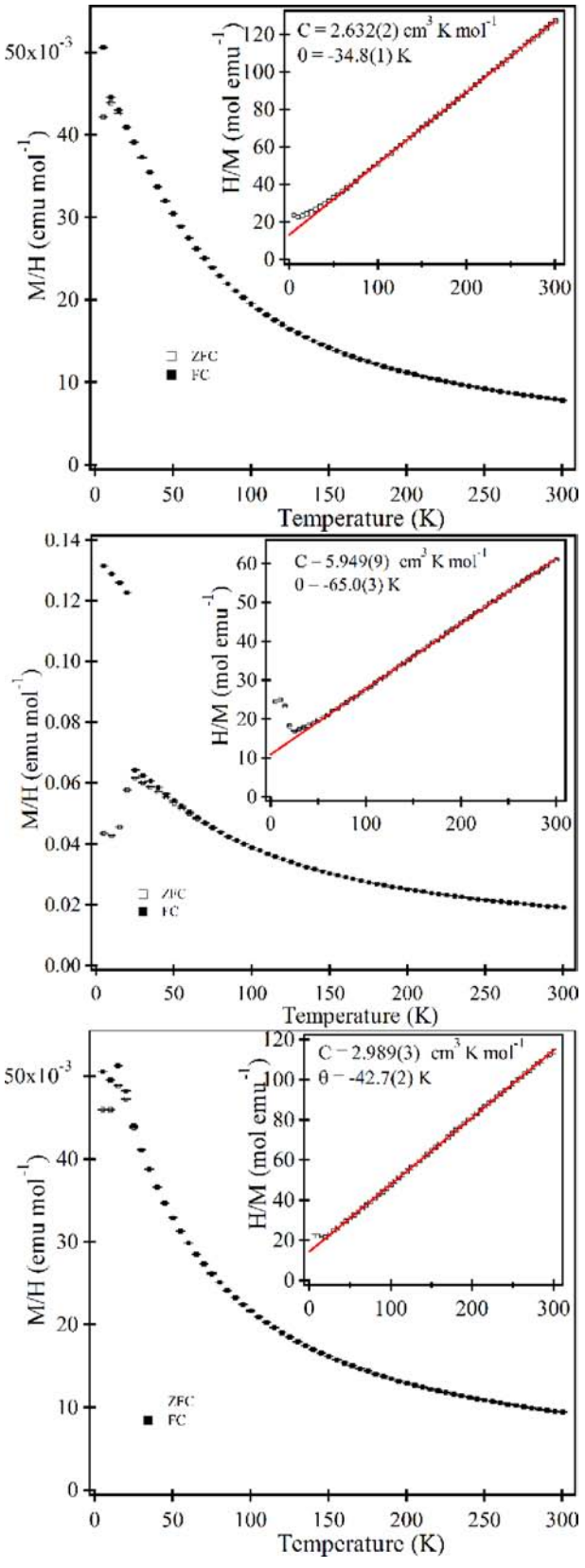

Figure 2. Zero field-cooled and field-cooled magnetization data collected as a function of temperature from Ba_2YCoO_5 (top), $Ba_3YCo_2O_{7.5}$ (middle), and $Ba_2YCoO_5F_{0.42}$ (bottom). Insets shows fits to the Curie–Weiss law.

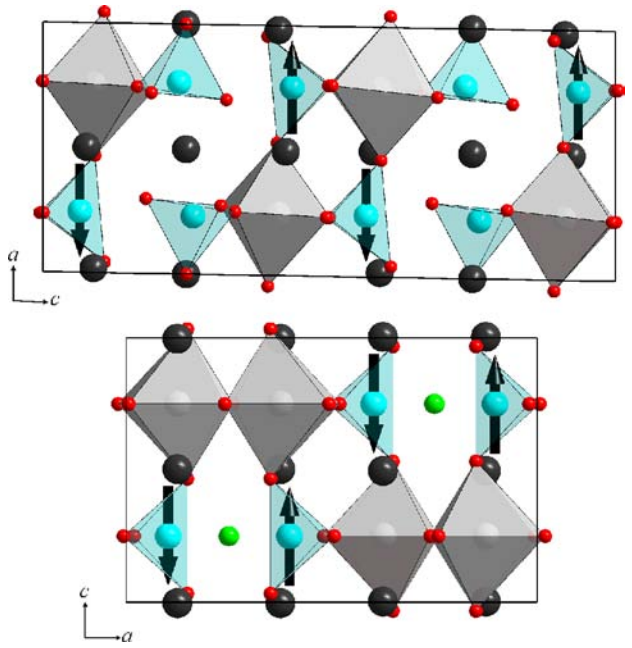

Figure 3. Magnetic structures of $Ba_3YCo_2O_{7.5}$ (top) and $Ba_2YCoO_5F_{0.42}$ (bottom). Gray octahedra represent YO_6, blue tetrahedra represent CoO_4, black spheres Ba^{2+} and green spheres F^-.

ordered magnetic structure of $Ba_3YCo_2O_{7.5}$ is shown in Figure 3 with complete details described in the Supporting Information.

$Ba_2YCoO_5F_{0.42}$. Magnetization data collected from $Ba_2YCoO_5F_{0.42}$ (Figure 2) can be fitted to the Curie–Weiss law in the temperature range $45 < T/K < 300$ to yield values of $C = 2.989(3)$ cm^3 K mol^{-1}, $\theta = -42.7(2)$ K,. broadly in agreement with a value of $C = 3.57$ cm^3 K mol^{-1} expected for the spin-only moment of a combination of high-spin Co^{3+} and high-spin Co^{4+} centers. Below this temperature zero field-cooled and field-cooled data diverge weakly. Neutron powder diffraction data collected from $Ba_2YCoO_5F_{0.42}$ at 7 K exhibit additional diffraction features compared to analogous data collected at ambient temperature, indicative of magnetic order. These additional diffraction features were readily indexed using the crystallographic unit cell. The intensities of these additional diffraction features are best described using an antiferromagnetic model, in which the magnetic moments of the cobalt centers in $Y_2Co_2O_{10}\square_2$ subunits are aligned parallel to the z-axis with an ordered moment of 0.95(8) μ_B per cobalt center, as shown in Figure 3, with complete details of the refined magnetic structure described in the Supporting Information.

DISCUSSION

Crystal Structures. Ba_2YCoO_5 and $Ba_3YCo_2O_{7.5}$ adopt anion-vacancy ordered, B-cation ordered perovskite structures directly analogous to the iron containing phases Ba_2YFeO_5 and $Ba_3YFe_2O_{7.5}$ respectively.[8] In common with the analogous iron phases, the ordered structures of Ba_2YCoO_5 and $Ba_3YCo_2O_{7.5}$ can be rationalized on the basis of the coordination preferences of Y^{3+} and Co^{3+} and the need to minimize the lattice strain which arises from the large mismatch in the ionic radii of the two B-cations (Y^{3+} 6CN = 0.90 Å, Co^{3+} 6CN = 0.61 Å).[21] By adopting the observed ordered structures the anion vacancies present in these phases are localized within the coordination sphere of the cobalt centers, rather than the yttrium centers,

dx.doi.org/10.1021/ic402349r | Inorg. Chem. 2013, 52, 13762–13769

and lattice strain is minimized by arranging the cobalt and yttrium cations into one-dimensional (1D) chains, rather than layered structures such as that of the $A_2B_2O_5$ brownmillerite structure, as discussed in detail previously.[8]

Both Ba_2YCoO_5 and $Ba_3YCo_2O_{7.5}$ contain Co^{3+} centers located within tetrahedral coordination sites. This is a rather unusual coordination geometry for Co^{3+} in extended oxides (octahedral or square-based pyramidal coordination is more typical).[22] The dearth of materials containing tetrahedrally coordinated Co^{3+} centers means there are no accurate ionic radii tabulated for 4 coordinate Co^{3+} hence the use of 6 coordinate radii in the discussion above.[21]

Examination of the BVS parameters calculated for the $Ba_nYCo_{n-1}O_{2.5n}$ phases (Tables 3 and 4) reveals that the yttrium centers are under compression (BVS > Y+3) and the cobalt centers are under tension (BVS < Co+3) consistent with the presence of considerable lattice strain. These deviations from expected BVS values are greater for the $Ba_nYCo_{n-1}O_{2.5n}$ series than the previously reported $Ba_nYFe_{n-1}O_{2.5n}$ series,[8] consistent with the smaller ionic radius of Co^{3+} compared to Fe^{3+} (Co^{3+} 6CN = 0.61 Å, Fe^{3+} 6CN = 0.64 Å).[21] The large lattice strain observed in cobalt and iron materials is also observed in structurally related $Ba_3ErGa_2O_{7.5}$ (BVS Er = +3.22; BVS Ga = +2.87, +2.75)[23] and suggests that the complex ordered structures adopted by $Ba_nREM_{n-1}O_{2.5n}$ (RE = Y; M = Fe, Co; n = 2, 3) phases are likely to be restricted to a limited number of RE^{3+}/M^{3+} combinations which lie in a relatively narrow range of "allowed" RE^{3+}:M^{3+} radius ratios.

Fluorine Insertion. Reaction of Ba_2YCoO_5 with CuF_2 under flowing oxygen results in oxidative topochemical insertion of fluoride ions, and the formation of the metastable phase $Ba_2YCoO_5F_{0.42}$. As discussed in more detail below, the insertion of fluoride ions into Ba_2YCoO_5 leads to only modest changes to the host structure. The largest structural effect of fluorination is a general contraction of both the YO_6 octahedra and CoO_4 tetrahedra which results in a straightening of the cooperatively twisted Y/Co−O polyhedral network. This can be most clearly seen in the linkages parallel to the z-axis, where the angle between oxide ions which connect the YO_6 octahedra and CoO_4 tetrahedra opens from O(1)−O(2)−O(1) = 165.11(7)° in Ba_2YCoO_5 to O(1)−O(1)−O(1) = 180.0° in $Ba_2YCoO_5F_{0.42}$. This contraction of the metal coordination polyhedra raises the calculated BVS of the yttrium cations from Y+3.32 to Y+3.45 indicating the YO_6 octahedra are becoming increasingly compressed, consistent with increasing lattice strain on fluorination. It is likely that it is this increase in lattice strain which limits the level of fluorine insertion to the observed $Ba_2YCoO_5F_{0.42}$ stoichiometry.

As shown in Table 6, the fluorine-cation bonds in $Ba_2YCoO_5F_{0.42}$ are longer than is typical in most metal fluorides. However fluoride ions have been observed in equally large, approximately octahedral coordination sites in transition metal oxyfluoride phases with Ruddlesden−Popper like structures, such as Sr_2FeO_3F and $Sr_2TiO_3F_{1.8}$.[19,24] It should be noted that the Co−F "bonds" present in $Ba_2YCoO_5F_{0.42}$ are sufficiently long (2.36(5) Å, 2.40(5) Å)) that it is reasonable to think that the fluoride ions are not in the primary coordination sphere of the cobalt cations. As a result the cobalt centers can still be considered tetrahedrally coordinated and no long-range Co−O/F-Co network is formed on fluorine insertion.

Strain Controlled Anion Insertion. As noted above, Ba_2YCoO_5 and Ba_2YFeO_5 have a direct isostructural relationship which makes it surprising that they exhibit strikingly different behavior under oxidizing conditions at low temperature. As anion "deficient" perovskite phases both Ba_2YCoO_5 and Ba_2YFeO_5 would be expected to undergo topochemical oxidative anion insertion, as is typical for phases of this type.[25] However unlike the majority of anion deficient perovskite phases, which tend to incorporate "additional" anions in a continuous way, the two Ba_2YMO_5 (M = Fe, Co) phases undergo rather specific oxidation reactions. Ba_2YFeO_5 reacts with 80 atm of oxygen at 410 °C to form the acentric phase $Ba_2YFeO_{5.5}$.[10] In contrast Ba_2YCoO_5 does not appear to undergo any topochemical anion insertion reaction with oxygen at ambient or high pressure (100 atm) but does incorporate fluorine to form $Ba_2YCoO_5F_{0.42}$.

The differing oxidation behavior of Ba_2YCoO_5 and Ba_2YFeO_5 can be rationalized by considering the structural consequences of oxidative anion insertion. As noted above, the large size mismatch between cobalt/iron and yttrium leads to a large lattice strain in the two B-cation ordered Ba_2YMO_5 phases. Insertion of additional anions will necessarily oxidize the transition metal M-cations driving a contraction of M-O bond lengths, leading to a further unfavorable increase in lattice strain which will limit or prevent topochemical anion insertion, unless some feature of the host lattice can relieve the strain in some way.

In the case of oxygen insertion into Ba_2YFeO_5, the increase in lattice strain on oxidation can be limited by organizing the inserted anions into an ordered layered arrangement.[10] When combined with a Jahn−Teller distortion of the resulting d^4 Fe^{4+} centers, the result is that half the iron centers reside in 5-coordinate square-based pyramidal sites, while the other half remain in tetrahedral sites. Critically these two features (ordered inserted anions and a Jahn−Teller distortion) mean that no long-range Fe−O−Fe network is formed on oxide insertion (Figure 4). This limits the lattice strain on oxidation as the presence of an Fe−O−Fe network would lead to intolerable lattice strain when combined with the existing Y−O−Y network because of the mismatch in Fe−O and Y−O bond lengths. Thus the Jahn−Teller distortion of Fe^{4+} centers can be seen as decisive in enabling the topochemical oxidation of Ba_2YFeO_5.

The lack of oxygen insertion into Ba_2YCoO_5 can be understood on a similar basis. While an ordered arrangement of inserted oxide ions analogous to that observed in $Ba_2YFeO_{5.5}$ could be formed within the Ba_2YCoO_5 host lattice, the Co^{4+} centers which would be formed on oxygen insertion would have a d^5 electronic configuration and would therefore not stabilize a Jahn−Teller driven structural distortion analogous to that seen in $Ba_2YFeO_{5.5}$. In the absence of such a distortion an extended Co−O−Co network of apex-linked CoO_6 centers would need to be formed on oxygen insertion which would require a dramatic contraction of the host lattice to accommodate the extended Co−O−Co network (Figure 4). The lack of oxygen insertion chemistry suggests that the lattice strain of such a hypothetical undistorted $Ba_2YCoO_{5.5}$ phase is too great and energetically unfavorable for the oxidation reaction to proceed.

In contrast to oxygen, fluorine can be readily inserted into Ba_2YCoO_5. Comparison of the structures of Ba_2YCoO_5 and $Ba_2YCoO_5F_{0.42}$ (Figure 5a and 5b) reveals that fluorination of Ba_2YCoO_5 perturbs the host structure very little. Figures 5c and 5d show the geometry around the "vacant" anion site at (0.25, 0, 0.25) in Ba_2YCoO_5 and the geometry of the fluoride ion site in $Ba_2YCoO_5F_{0.42}$, respectively. It can be seen that with the exception of a little relaxation, related to the contraction and

dx.doi.org/10.1021/ic402349r | Inorg. Chem. 2013, 52, 13762−13769

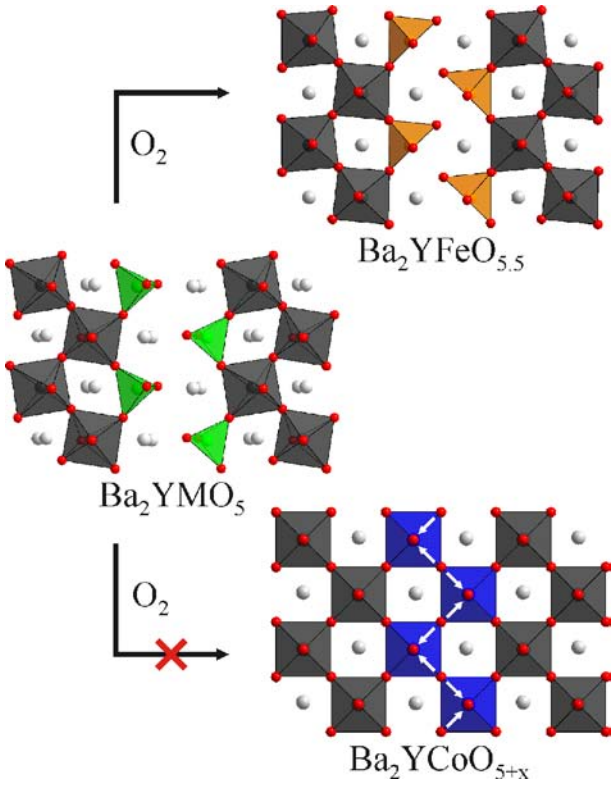

Figure 4. Insertion of oxygen into Ba_2YFeO_5 leads to $Ba_2YFeO_{5.5}$. In contrast, Ba_2YCoO_5 does not intercalate oxygen because the lattice strain of the resulting Ba_2YCoO_{5+x} phase makes this process unfavorable.

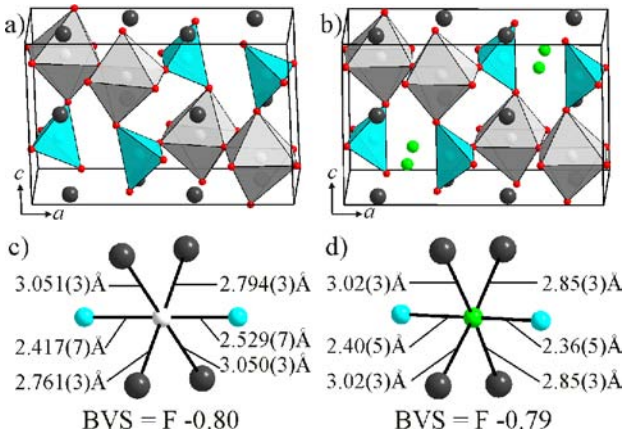

Figure 5. Comparison of the structures of (a) Ba_2YCoO_5 and (b) $Ba_2YCoO_5F_{0.42}$. (c) The "vacant" anion site in Ba_2YCoO_5 and (d) the local coordination polyhedron of fluoride ions in $Ba_2YCoO_5F_{0.42}$. Black spheres represent Ba^{2+}, blue spheres/polyhedra cobalt centers, gray spheres/polyhedra Y^{3+}, and green spheres F^-.

twisting of the CoO_4 and YO_6 polyhedra on oxidation, the two sites are very similar. Significantly the two sites have almost identical BVS values, indicating there is no large scale contraction of the site associated with fluorine insertion. Thus the insertion of fluorine into Ba_2YCoO_5 proceeds because the vacant anion sites within the host phase are already a suitable size and shape to accommodate the inserted fluoride ions without perturbing the host lattice significantly.

The modest structural perturbation observed on fluorine insertion suggests the inserted fluoride ions may exhibit reasonable mobility at modest temperatures. To date no ionic transport measurements have been performed on $Ba_2YCoO_5F_{0.42}$, but given the low synthesis temperature at which fluorine is inserted (275 °C) and the generally good ionic conductivity observed from metal fluorides,[26,27] it is reasonable to think that $Ba_2YCoO_5F_{0.42}$ could exhibit good fluoride ion conductivity.

Magnetic Behavior. The low-temperature magnetic behavior of the three Ba−Y−Co-O/F phases varies to a reasonable extent. Ba_2YCoO_5 exhibits paramagnetic behavior down to the lowest temperature of the three Ba−Y−Co-O/F phases (40 K) and shows no sign of long-range magnetic order. In comparison $Ba_3YCo_2O_{7.5}$ and $Ba_2YCoO_5F_{0.42}$ deviate from Curie−Weiss behavior at 65 and 45 K respectively, and both phases exhibit long-range antiferromagnetic order at low temperature. These observations indicate that the superexchange coupling present in Ba_2YCoO_5 is considerably weaker than that in either $Ba_3YCo_2O_{7.5}$ or $Ba_2YCoO_5F_{0.42}$. Examination of the crystal structures of the three phases reveals that Ba_2YCoO_5 has the smallest average Co−O−Y bond angle at 156.2°, compared to 163.2° and 162.9° for $Ba_3YCo_2O_{7.5}$ and $Ba_2YCoO_5F_{0.42}$ respectively, which is entirely consistent with the observed trend in superexchange coupling strength.[28] In addition the oxidation of some Co^{3+} to Co^{4+} in $Ba_2YCoO_5F_{0.42}$ is also expected to increase the strength of superexchange coupling in this phase.[2] The proximity of the magnetic ordering temperatures of $Ba_3YCo_2O_{7.5}$ and $Ba_2YCoO_5F_{0.42}$ to the temperature at which the neutron diffraction data were collected (7 K) make it hard to draw conclusions based on the size of the ordered moments observed for either phase.

CONCLUSION

The complex cation-ordered, anion-vacancy ordered phases Ba_2YCoO_5 and $Ba_3YCo_2O_{7.5}$ have been prepared and shown to have structures which are analogous to the corresponding iron phases Ba_2YFeO_5 and $Ba_3YFe_2O_{7.5}$.[8] Investigation of the oxidative insertion chemistry of Ba_2YCoO_5 reveals it does not incorporate oxygen even under a pressure of 100 atm, yet readily intercalates fluorine to form $Ba_2YCoO_5F_{0.42}$. This selective insertion of fluorine rather than oxygen is in contrast to the iron analogue Ba_2YFeO_5, which is topochemically oxidized under 80 atm of oxygen pressure to form $Ba_2YFeO_{5.5}$.[10] This difference in intercalation behavior can be understood on the basis of lattice strain and the Jahn−Teller instability of octahedral d^4 Fe^{4+} centers.

The observation that structural and chemical features of can change the intercalation behavior of these cation-ordered anion-vacancy ordered host phases so dramatically suggests that with suitable chemical substitution the "chemical" behavior of such phases could be tuned for use in applications such as oxygen storage/separation or as electrolytes or electrodes in fuel cells or anion shuttle battery systems. Indeed, the observed selective intercalation of fluorine over oxygen could, in principle, improve the oxygen tolerance of recently demonstrated fluoride ion shuttle battery systems,[29] if Ba_2YCoO_5 was employed as an anode, by preventing undesirable oxidation by aerial oxygen.

ASSOCIATED CONTENT

Supporting Information

A diagram and description on the apparatus used to fluorinate Ba_2YCoO_5 with physically separated CuF_2. Observed, calculated, and difference plots from the room-temperature

dx.doi.org/10.1021/ic402349r | Inorg. Chem. 2013, 52, 13762−13769

structural refinements of Ba_2YCoO_5, $Ba_3YCo_2O_{7.5}$, and $Ba_2YCoO_5F_{0.42}$. Refined parameters and observed, calculated, and difference plots from the nuclear and magnetic refinements of $Ba_3YCo_2O_{7.5}$ and $Ba_2YCoO_5F_{0.42}$. This material is available free of charge via the Internet at http://pubs.acs.org.

AUTHOR INFORMATION

Corresponding Author

*E-mail: michael.hayward@chem.ox.ac.uk. Phone: +44 1865 272623. Fax: +44 1865 272690.

Author Contributions

The manuscript was written through contributions of all authors.

Notes

The authors declare no competing financial interest.

ACKNOWLEDGMENTS

We thank W. Kockelmann for assistance collecting the neutron powder diffraction data. Experiments at the ISIS pulsed neutron facility were supported by a beam time allocation from the Science and Technology Facilities Council. K.L. thanks the Pacific Alliance Group for a scholarship. P.S.H. and T.T.T. thank the Robert A. Welch Foundation (Grant E-1457) for support.

REFERENCES

(1) Cooper, S. L.; Egami, T.; Goodenough, J. B.; Zhou, J.-S. *Localized to Itinerant Electronic Transition in Perovskite Oxides*; Springer-Verlag: Berlin, Germany, 2001.

(2) Goodenough, J. B. *Prog. Solid State. Chem.* **1971**, *5*, 149.

(3) King, G.; Woodward, P. M. *J. Mater. Chem.* **2010**, *20*, 5785.

(4) Anderson, M. T.; Greenwood, K. B.; Taylor, G. A.; Poeppelmeier, K. R. *Prog. Solid State Chem.* **1993**, *22*, 197.

(5) Meneghini, C.; Sugata, Ray; Liscio, F.; Bardelli, F.; Mobilio, S.; Sarma, D. D. *Phys. Rev. Lett.* **2009**, *103*, 46403.

(6) Antipov, E. V.; Abakumov, A. M.; Istomin, S. Y. *Inorg. Chem.* **2008**, *47*, 8543.

(7) Turp, S. A.; Hargreaves, J.; Baek, J.; Halasyamani, P.; Hayward, M. A. *Chem. Mater.* **2010**, *22*, 5580.

(8) Luo, K.; Hayward, M. A. *Inorg. Chem.* **2012**, *51*, 12281.

(9) Yang, T.; Claridge, J. B.; Rosseinsky, M. J. *Inorg. Chem.* **2013**, *52*, 3795.

(10) Luo, K.; Johnson, R. D.; Tran, T. T.; Halasyamani, P. S.; Radaelli, P. G.; Hayward, M. A. *Chem. Mater.* **2013**, *25*, 1800.

(11) Li, R. K.; Greaves, C. *Phys. Rev. B* **2000**, *62*, 3811.

(12) Larson, A. C.; Von Dreele, R. B. *General Structure Analysis System (GSAS)*; Los Alamos National Laboratory Report LAUR 86-748; Los Alamos National Laboratory: Los Alamos, NM, 2000.

(13) Kurtz, S. K.; Perry, T. T. *J. Appl. Phys.* **1968**, *39*, 3798.

(14) Rieckhof, K. E.; Peticola, W. l. *Science* **1965**, *147*, 610.

(15) Ok, K. M.; Chi, E. O.; Halasyamani, P. S. *Chem. Soc. Rev.* **2006**, *35*, 710.

(16) Sears, V. F. *Neutron News* **1992**, *3*, 26.

(17) *International Tables for Crystallography*: Kluwer Academic Publishers: Dordrecht, The Netherlands, 2002; Vol. *A*.

(18) Brese, N. E.; O'Keeffee, M. *Acta Crystallogr., Sect. B: Struct. Sci.* **1991**, *B47*, 192.

(19) Case, G. S.; Hector, A. L.; Levason, W.; Needs, R. L.; Thomas, M. F.; Weller, M. T. *J. Mater. Chem.* **1999**, *9*, 2821.

(20) Romero, F. D.; Bingham, P. A.; Forder, S. D.; Hayward, M. A. *Inorg. Chem.* **2013**, *52*, 3388.

(21) Shannon, R. D. *Acta Crystallogr.* **1976**, *A32*, 751.

(22) Raveau, B.; Seikh, M. M. *Cobalt oxides: from crystal chemistry to physics*; Wiley-VCH Verlag: Weinhei, Germany, 2012.

(23) Abakumov, A. M.; Shpanchenko, R. V.; Lebedev, O. I.; Van Tendeloo, G.; Amelinckx, S.; Antipov, E. V. *Acta Crystallogr., Sect. A* **1999**, *55*, 828.

(24) Slater, P. R.; Gover, R. K. B. *J. Mater. Chem.* **2002**, *12*, 291.

(25) Hayward, M. A. In *Comprehensive Inorganic Chemistry II*; Reedijk, J., Poeppelmeier, K. R., Eds.; Elsevier: Oxford, U.K., 2013; Vol. *2*, p 417.

(26) Hagenmuller, P.; Reau, J. M.; Lucat, C.; Matar, S.; Villeneuve, G. *Solid State Ionics* **1981**, *3*−*4*, 341.

(27) Patro, L. N.; Hariharan, K. *Solid State Ionics* **2013**, *239*, 41.

(28) Goodenough, J. B. *Magnetism and the Chemical Bond*; Wiley: New York, 1963.

(29) Reddy, M. A.; Fichtner, M. *J. Mater. Chem.* **2011**, *21*, 17059.